分类号_____　　密级

U D C_____　　编号

中国科学院地球化学研究所

博 士 后 研 究 工 作 报 告

Use of both Hg and S-Mass Independent Fractionation on aerosols to constrain the formation of both Particles-Bound Mercury (PBM) and sulfates in the atmosphere

David AU YANG

工作完成日期　2018 年 4 月—2020 年 3 月

报告提交日期　　2020 年 4 月

中国科学院地球化学研究所 （贵阳）

2020 年 4 月

Use of both Hg and S-Mass Independent Fractionation on aerosols to constrain the formation of both Particles-Bound Mercury (PBM) and sulfates in the atmosphere

博 士 后 姓 名 **David AU YANG**

流动站（一级学科）名称 中国科学院地球化学研究所

专 业（二级学科）名称 环境地球化学

研究工作起始时间 2018 年 4 月 01 日

研究工作期满时间 2020 年 3 月 31 日

中国科学院地球化学研究所 （贵阳）

2020 年 4 月

声 明

本人声明所呈交的博士后出站报告是我个人和合作导师指导下进行的研究工作及取得的研究成果。尽我所知，除文中特别加以标注和致谢的地方外，论文中不包含其他人已经发表或撰写过的研究成果，也不包含为获得中国科学院地球化研究所或其他教育机构和科研单位的学位或证书而使用过的材料。与我一同工作的同志对本研究所做的任何贡献均已在论文中作了明确说明并表示了谢意。

签名：_____日期：2020 年 3 月 31 日

关于博士后出站报告使用授权说明

本人完全了解中国科学院地球化学研究所有关保留、使用博士后出站报告的规定，即中国科学院地球化学研究所有权保留送交博士后出站报告的复印件，允许博士后研究报告被查阅和借阅；中国科学院地球化学研究所可以公布博士后研究报告的全部或部分内容，可以采用影印、缩印或其他复制手段保存研究报告。

☑公开 □保密（__年）（保密的论文在解密后应遵守此规定）

博士后签名：_____

合作导师签名：_____

日期：2020 年 3 月 31 日

Abstract

Both Mercury (Hg) and Sulfur (S) are ubiquitous elements in the aerosols present as Particle-Bound Mercury (PBM) and sulfate. Constraining both sources and atmospheric processes affecting the budget for both Hg and S in the aerosols are important regarding their impacts on the atmosphere and Human health. This could be achieved using the multiple isotopic compositions for both elements which have been shown to be powerful sources and processes tracers in others environments.

We first investigated the sources and processes affecting both the Hg and S in marine aerosols collected shipboard showing that Hg and S isotopic compositions would not be explained by a mixing between sources but would rather be explained by atmospheric processes. We then investigate the sources and processes responsible for the Hg isotopic compositions measured in Montréal over the year 2015 in two different stations, one urban and one subrural stations. We identified three possible sources and suspect the implication of an additional atmospheric process responsible for such isotopic signatures. We finally measured the S isotopic compositions in aerosols collected in Tianjin and discussed about the potential contributions of sources and atmospheric processes.

Keywords : Multiple isotopic compositions, sulfur, mercury, aerosols, processes, sources

Table of Materials

1 Introduction 7
2 Materials and methods 10
2.1 S multi-isotope analysis 10
2.2 Hg multi-isotope analysis 10
2.3 Major elements concentrations 11
2.4 HYSPLIT Calculation 11
3 Hg and S isotopic compositions in marine aerosols 11
3.1 Hg Results and comparison with literature data 11
3.2 S isotopic compositions results and comparison with literature data 12
4 Hg isotopic compositions in an rural and subrural areas 14
4.1 Sampling strategy 14
4.2 Results and Comparison with literature data 14
5 S isotopic compositions in an urban area 16
5.1 Sampling strategy 16
5.2 S isotopic compositions results and comparison with literature data 16
6 Supplementary activities 16
6.1 Publications of the thesis papers (1st author and 2nd author) 16
6.2 Publication of papers as coauthor 18
6.3 Reviewing papers 18
6.4 Meeting 18
7 Reference 19

Table of Figures

Figure 1: Mercury isotopic compositions in aerosols in a δ^{202}Hg-Δ^{201}Hg diagram, δ^{202}Hg-Δ^{200}Hg diagram and in a δ^{202}Hg-Δ^{199}Hg diagram. Different types of aerosols reported in the literature are also shown..... 12

Figure 2 : Sulfur isotopic compositions in a δ^{34}S-Δ^{33}S diagram and in a Δ^{33}S-Δ^{36}S diagram. Urban aerosols have also been reported*(Au Yang et al., 2019; Guo et al., 2010; Lin et al., 2018b; Romero and Thiemens, 2003; Shaheen et al., 2014)*. No Δ^{33}S and Δ^{36}S-values have been reported to our knowledge for marine aerosols. Slopes for the different atmospheric processes (photooxidation, photolysis, self-shielding), Archean slope and Phanerozoic slopes have also been reported..... 13

Figure 3: Odd-MIF and even-MIF time series in aerosols sampled in Montreal. Locally weighted scatter plot smoothing (LOWESS) for all the Hg isotopic compositions are also shown 15

Figure 4 : Variations of (A) Δ^{199}Hg and (B) Δ^{200}Hg as a function of δ^{202}Hg in PBM from PM_{10} aerosols collected in Montreal (purple square and green diamond). Light gray, gray and black dots represent Hg isotopic compositions reported for aerosols from the literatures (Das et al., 2016; Fu et al., 2019; Huang et al., 2016; Huang et al., 2019; Huang et al., 2015; Huang et al., 2018; Rolison et al., 2013; Xu et al., 2017; Xu et al., 2019; Yu et al., 2016; Yuan et al., 2018) 15

Figure 5 Sulfur isotopic compositions in a δ^{34}S-Δ^{33}S diagram and in a Δ^{33}S-Δ^{36}S diagram. Urban aerosols have also been reported (Au Yang et al., 2019; Guo et al., 2010; Han et al., 2017b; Lin et al., 2018b; Romero and Thiemens, 2003; Shaheen et al., 2014) 16

1 Introduction

Mercury (Hg) is a toxic element that has the ability to recycle, at a large scale, in the atmosphere following successive oxidation and reduction reactions. As the Hg main form, elemental mercury (Hg^0) is relatively stable and has a lifetime of 0.5 to 1 year that allows it to be transported over long distances worldwide (Selin, 2009). Hg^0 can be oxidized into reactive mercury (Hg^{II}) via several possible pathways (see Si and Ariya (2018) review) which could be incorporated into particles (particles bound mercury PBM). Upon deposition, Hg^{II} could be photoreduced back to Hg^0 or transformed into methylmercury which can be bioaccumulated in living aquatics organism and thus impacting the Human health (Giang and Selin, 2016; Walters et al., 2015). This emphasizes the need to better constrain the different oxidation pathways that Hg^0 undergoes.

However, the dominant oxidation mechanisms for atmospheric Hg are still in debate. Possible oxidants include OH and O_3, which are the main sources of tropospheric oxidization capacity and which have been suggested to be important Hg^0 oxidants (Bieser et al., 2017; Cohen et al., 2004; De Simone et al., 2015; Gencarelli et al., 2014; Travnikov et al., 2017). Halogen species (mainly Br) are also found to be able to quickly oxidize Hg^0 during atmospheric mercury depletion event (AMDEs) in both Arctic and Antarctic spring when atmospheric Br concentrations are high. This Hg oxidation pathway which has been suggested to be the major one worlwide would involve a two-step oxidation with a first step involving an Br· or Cl· atom forming an intermediate Hg species (Hg^I) (Horowitz et al., 2017; Si and Ariya, 2018; Sun et al., 2016) and a second step oxidation involving NO_2, HO_2, BrO, ClO, IO into Hg^{II} (Dibble et al., 2012). Atmospheric models that considered distinct Hg^0 oxidants (i.e. Br/Cl or OH/ O_3) both showed results in good agreement with the observed Hg^0 concentration and wet deposition flux (De Simone et al., 2015; Horowitz et al., 2017; Travnikov et al., 2017), suggesting that currently available observations cannot constrain the main Hg^0 oxidation pathway .

Another biogeochemical cycle which is important to constrain is the sulfur (S) cycle due to it impacts on the atmosphere. Sulfates, which could result from the oxidation of SO_2 and DMS (dimethylsulfide) following two major chemical oxidation pathways (gaseous and aqueous), play a key role on the climate change and air pollution (Albrecht, 1989; Lelieveld et al., 2015; Levy et al., 2013; Myhre et al., 2013; Penner et al., 1992; Penner et al., 2006; Ramanathan et al., 2005; Ramanathan et al., 2001). More specifically SO_2 aqueous phase oxidation which occurs via several possible oxidants (i.e. O_2+TMI (Transition Metal Ion), H_2O_2, O_3 and NO_2 (Alexander et al., 2012; Alexander et al., 2009; Cheng et al., 2016; Harris et al., 2013a; Harris et al., 2013b; Herrmann, 2003; Lee and Schwartz, 1983; Sarwar et al., 2013; Seinfeld and Pandis, 2012)) produces sulfates which will be released during the evaporation of cloud water. These sulfates will condense on pre-existing and different sizes particles present in the cloud droplets (Mertes et al., 2005a; Mertes et al., 2005b). This would have the effect of reducing the radiative impact of sulfate aerosols. On the other hand, gaseous phase oxidation, which occurs predominantly via OH, leads to the formation of new sulfate particles by homogeneous nucleation process (Benson, 2008; Kulmala et al., 2004; Tanaka et al., 1994). Thus, sulfates resulting from which oxidation pathways it undergoes will induce different effect on the atmosphere.

However, both elements are considered relevant anthropogenic tracers and the use of their isotopes could help to constrain their oxidation pathways. Both Hg and S have multiple isotopes; the mercury has seven isotopes, ^{196}Hg, ^{198}Hg, ^{199}Hg, ^{200}Hg, ^{201}Hg, ^{202}Hg and ^{204}Hg whose abundances are 0.15%, 10%, 16.94%, 23.14%, 13.17%, 29.74% and 6.82% while sulfur has four stable isotopes, ^{32}S, ^{33}S, ^{34}S and ^{36}S whose natural abundances are approximately 95%, 0.75%, 4.2% and 0.015%, respectively (Ding et al., 2001). For both systems, the isotopic compositions are expressed by δ-notation. In particular, Hg-isotopic compositions are expressed as (Blum and Bergquist, 2007):

$$\delta^{xxx}\mathrm{Hg} = \left(\frac{\left({}^{xxx}\mathrm{Hg} / {}^{198}\mathrm{Hg} \right)_{\mathrm{sample}}}{\left({}^{xxx}\mathrm{Hg} / {}^{198}\mathrm{Hg} \right)_{\mathrm{NIST\ 3133}}} \right) - 1$$

where ^{xxx}Hg is one of the Hg heavy isotopes (^{199}Hg, ^{200}Hg, ^{201}Hg, ^{202}Hg and ^{204}Hg). NIST 3133 is the international mercury standard. In a similar way, the S-isotopic compositions are expressed as:

$$\delta^{3x}\mathrm{S} = \left(\frac{\left({}^{3X}\mathrm{S} / {}^{32}\mathrm{S} \right)_{\mathrm{sample}}}{\left({}^{3X}\mathrm{S} / {}^{32}\mathrm{S} \right)_{\mathrm{CDT}}} \right) - 1$$

where ^{3x}S is one of the S heavy isotopes (^{33}S, ^{34}S or ^{36}S) and CDT is the Vienna Canyon Diablo Troilite ^{34}S/^{32}S international standard. There is no international standard for the ^{33}S/^{32}S and ^{36}S/^{32}S. Accuracy of the measured values is established by direct comparison with data measured by other laboratories.

Generally, the multiple isotope ratios in each system (i.e. Hg and S respectively) are scaled to each other according to their mass $((1/m_1-1/m_2)/(1/m_1-1/m_3))$, following a "mass-dependent fractionation" model (Farquhar et al., 2000). For example, for the S, the isotope fractionation of ^{33}S over ^{32}S (1 amu difference) has approximately half the magnitude of the fractionation of the ^{34}S over ^{32}S (2 amu difference). More rigorously, mass-dependent fractionation is expressed by (Dauphas and Schauble, 2016; Young et al., 2002):

$$^{y}\alpha = (\ ^{x}\alpha)^{y\beta}$$

Where for the Hg system, ^{x}α is ^{202}α, ^{y}α is either ^{199}α, ^{200}α, ^{201}α or ^{204}α and ^{y}β is either ^{199}β, ^{200}β, ^{201}β or ^{204}β while for the S system ^{x}α is ^{34}α, ^{y}α is either ^{33}α or ^{36}α and ^{y}β is either ^{33}β or ^{36}β. The ^{y}β-exponent describes the relative fractionation of ^{y}Hg/^{198}Hg and ^{x}Hg/^{198}S for the Hg system it describes the relative fractionation of ^{y}S/^{32}S and ^{x}S/^{32}S for the S system. Its value depends on the reaction considered (Farquhar et al., 2001; Harris et al., 2013a; Ono et al., 2013; Watanabe et al., 2009). At high temperature, ^{199}β, ^{200}β, ^{201}β and ^{204}β-values are respectively 0.252, 0.502, 0.752 and 1.492 respectively (Blum and Bergquist, 2007). These deviations of the ^{3y}β-value from these high temperature values are expressed as follows and called mass independent fractionation (MIF):

$$\Delta^{199}Hg = \left(\delta^{202}Hg + 1\right) - \left(\delta^{202}S + 1\right)^{0.252}$$

$$\Delta^{200}Hg = \left(\delta^{202}Hg + 1\right) - \left(\delta^{202}S + 1\right)^{0.502}$$

$$\Delta^{201}Hg = \left(\delta^{202}Hg + 1\right) - \left(\delta^{202}S + 1\right)^{0.752}$$

$$\Delta^{204}Hg = \left(\delta^{202}Hg + 1\right) - \left(\delta^{202}S + 1\right)^{1.492}$$

At high temperature (> 500°C), the $^{33}\beta$ and $^{36}\beta$ -values are respectively 0.515 and 1.889 (Eldridge et al., 2016; Otake et al., 2008). Deviation of the $^{3y}\beta$-value from these high temperature values usually leads to non-zero $\Delta^{33}S$ and $\Delta^{36}S$ values typically in the range of ±0.1‰ and ±1‰, respectively. $\Delta^{33}S$ and $\Delta^{36}S$ are expressed as follows (Farquhar and Wing, 2003):

$$\Delta^{33}S = \left(\delta^{33}S + 1\right) - \left(\delta^{34}S + 1\right)^{0.515}$$

$$\Delta^{36}S = \left(\delta^{36}S + 1\right) - \left(\delta^{34}S + 1\right)^{1.889}$$

Both Hg and S isotopes have been shown to be good tracers of atmospheric processes as they are sensitive to the different oxidation pathways they undergo (Au Yang et al., 2018; Harris et al., 2013a; Sun et al., 2016). However, the observation of aerosols collected in various environments characterized by $\Delta^{199}Hg$ varying from -1.50 to 1.50‰, $\Delta^{200}Hg$ varying from -0.20 to 1.20‰ and $\Delta^{201}Hg$ varying from -1.50 to 1.50‰ remain unexplained (Das et al., 2016; Fu et al., 2019; Huang et al., 2019; Rolison et al., 2013; Xu et al., 2017; Xu et al., 2019; Yu et al., 2016). Odd-MIF (i.e. $\Delta^{199}Hg$ and $\Delta^{201}Hg$) are likely related to the magnetic isotope effect (MIE) and the nuclear volume effect (NVE) (Bergquist and Blum, 2007; Buchachenko, 2013; Cai and Chen, 2016) and are mainly observed during photochemical reduction of Hg^{2+}, MeHg photo-demethylation, abiotic dark reduction and liquid-vapor evaporation (Bergquist and Blum, 2007; Estrade et al., 2009; Zheng and Hintelmann, 2009, 2010). On the other hand, the mechanism triggering even-MIF (i.e. $\Delta^{200}Hg$ and $\Delta^{204}Hg$) that are reported in many atmospherically related samples (Chen et al., 2012; Sherman et al., 2010; Wang et al., 2015; Yuan et al., 2018; Yuan et al., 2015) remains unknown, although some studies suggested that it might be related to photochemical oxidation of elemental Hg^0 in the tropopause (Chen et al., 2012) or to specific reactions (e.g. self shielding effect in compact fluorescent lamp; (Mead et al., 2013)). More recently, Sun et al. (2016) also suggested that the oxidation of Hg^0 by halogen atoms also produces both odd- and even-MIF. Therefore, oxidation reactions have also the potential to trigger MIF in Hg isotopes, especially in atmospheric samples such as aerosols.

In another hand, modern aerosols are characterized by $\Delta^{33}S$-values varying from -0.6 to 0.5‰ (Au Yang et al., 2019; Guo et al., 2010; Han et al., 2017a; Lin et al., 2018b; Romero and Thiemens, 2003; Shaheen et al., 2014). Origins of such small but significant positive $\Delta^{33}S$-anomalies remain poorly constrained but they could result either from sulfate stratospheric aerosol (SSA) inputs and/or secondary sulfates formed during SO_2 oxidation (Au Yang et al., 2019; Guo et al., 2010; Han et al., 2017b; Harris et al., 2013a; Romero and Thiemens, 2003; Shaheen et al., 2014). Origin of such negative $\Delta^{33}S$-values down to -0.6‰ remains even more speculative where it has been suggested to reflect input of sulfur from incomplete combustion reactions (Han et al., 2017b; Lin et al., 2018a) in particular in residential stoves during winter in Beijing (Han et al., 2017b).

Thus, due to the similarities between Hg and O or S (i.e. oxidation of a gaseous phase by OH, O_3, and halogens, presence of MIF associated to the oxidation pathway and presence of S and Hg-MIF in aerosols which remains unexplained), coupling these isotopic systems would share complementary information on the atmospheric oxidation mechanisms and provide constrain on the different Hg^0 and SO_2 oxidation pathways although those isotopic compositions are usually analyzed separately because both sulfate/nitrate and Hg^{II} have different baring-minerals within the aerosols and are usually not correlated (Beddows et al., 2004).

2 Materials and methods

2.1 S multi-isotope analysis

Aerosols filters were inserted into a reaction vessel heated at 180°C with 20 mL of Thode solution, a mixture of hydrochloric, hydroiodic and hypophosphorous acids (Thode et al., 1961), for 1.3 hours to quantitatively reduce sulfate into H_2S. The formed gases were purged from the vessel using nitrogen gas, bubbled through deionized water and subsequently passed through a 0.3 M silver nitrate ($AgNO_3$) solution to form silver sulfide (Ag_2S). This solid Ag_2S was then rinsed twice with Millipore water and dried at 70°C overnight. Ag_2S was then loaded into an aluminum foil, weighted and degassed under vacuum.

Ag_2S was subsequently converted to SF_6 by reacting with approximately 200 Torr of excess fluorine in a nickel bomb at 250°C. The produced SF_6 was purified using both cryogenic techniques and gas chromatography, quantified and subsequently analyzed by dual inlet isotope ratio mass spectrometry (Thermo-Fisher MAT-253) where m/z = 127, 128, 129 and 131 ion beams were monitored.

The $\delta^{34}S$-values were measured against our in-house SF_6 tank that had been previously calibrated with respect to the IAEA-S1 international standards and expressed versus V-CDT assuming a $\delta^{34}S_{S1}$= -0.3‰ vs V-CDT isotope composition. To express our $\Delta^{33}S$ and $\Delta^{36}S$ data with respect to V-CDT, we anchored our data using CDT-data measured previously in the laboratory following Defouilloy et al. (2016). No further corrections were carried out, other than normalization of the data to CDT. $\Delta^{33}S$ and $\Delta^{36}S$ IAEA-standards were within values reported elsewhere (Au Yang et al., 2016; Defouilloy et al., 2016; Labidi et al., 2012). Our analysis (n = 5) of IAEA-S1 standard yielded: $\delta^{34}S$ = -0.33 ± 0.02‰(2σ), $\Delta^{33}S$ = 0.074 ± 0.010‰(2σ) and $\Delta^{36}S$ = -0.8 ± 0.2‰(2σ) vs CDT. Analyses of the international sulfate standard NBS-127 was also performed and gave a $\delta^{34}S$ of 20.8 ± 0.4‰ (2σ; n = 12), consistent with the 20.3 ± 0.4‰ value reported by the IAEA.

2.2 Hg multi-isotope analysis

Aerosol filters were combusted using the dual-stage protocol described in Huang et al. (2015) to concentrate Hg. Briefly, each filter was introduced into a quartz tube that then underwent two successive combustions at 950°C, followed by a combustion at 1000°C for a total time of 3.5h to decompose the Hg^{II} present under the form of Hg_p into vapor Hg^0 (Sun et al., 2013). The combustion products, Hg^0 and other compounds, were purged using Hg-free O_2, and bubbled through a 5mL HNO_3-HCl-H_2O mixture

(2:4:9) acid trap (Huang et al., 2015; Sun et al., 2013). The generated solution was then transferred into a pre-cleaned glass bottle. 50µL of 0.2M BrCl were then added to convert Hg^0 into Hg^{II}.

Hg^{II} was then converted back into Hg^0 by reacting with $SnCl_2$ and injected into a multi-collector inductively coupled plasma mass spectrometer (Neptune plus) simultaneously with Tl, which was used as an internal standard to correct for the instrumental mass bias (Blum and Bergquist, 2007; Yin et al., 2016). A high concentration of Tl (20ppb) was injected with each sample to prevent the formation of Hg hybrids during the analysis (Yin et al., 2016). The faraday cups were positioned to collect ^{198}Hg (L3), ^{199}Hg (L2), ^{200}Hg (L1), ^{201}Hg (C), ^{202}Hg (H1), ^{203}Tl (H2) and ^{205}Tl (H3). Hg multi-isotope compositions were then determined by standard bracketing using the Hg NIST 3133 international standard. The NIST 3177 standard was also regularly analyzed with concentrations matching those of the aerosol samples (i.e. 2 ppb) to test the instrument stability and to control the measurement quality (Geng et al., 2018). Repeated analyses (n=22) of the NIST 3177 standard gave $\delta^{202}Hg$ = -0.52 ± 0.03‰ (2σ), $\Delta^{199}Hg$ = -0.02 ± 0.05‰ (2σ), $\Delta^{200}Hg$ = 0.01 ± 0.03‰ (2σ), $\Delta^{201}Hg$ = -0.01 ± 0.02‰ (2σ) vs NIST 3133, consistent with previous reported values (Chen et al., 2016; Fu et al., 2019; Sun et al., 2016; Wang et al., 2015; Yuan et al., 2018; Zhang et al., 2020). Analysis of a second certified reference material CRM024 (n=8) gave $\delta^{202}Hg$ = -1.43 ± 0.08‰ (2σ), $\Delta^{199}Hg$ = 0.03 ± 0.02‰ (2σ), $\Delta^{200}Hg$ = -0.00 ± 0.02‰ (2σ), $\Delta^{201}Hg$ = 0.00 ± 0.01‰ (2σ) vs NIST 313, consistent isotope compositions reported by Huang et al. (2015).

2.3 Major elements concentrations

Concentrations of selected soluble inorganic species (Na^{2+}, K^+, Ca^{2+}, Mg^{2+}, NO_3^-, SO_4^{2-}, Cl^-) were measured using a Dionex®ICS-90 and a Vista MPX Varian ICP-OES after extraction from a 3 cm x 3 cm filter piece in 30 mL Milli-Q water (Paris et al., 2010). Detection limits for these ionic species were usually in the order of 5 $\mu g.L^{-1}$, i.e. 0.1 $ng.m^{-3}$ considering our sampling and extraction protocols. Hg concentrations were measured by cold vapor atomic fluorescence spectroscopy (CVAFS, Tekran 2500) after reducing an aliquot of the pre-concentrated Hg^{II} into Hg^0 using $SnCl_2$. The Hg^0 was then collected on a gold-coated bead trap and analyzed with the CVAFS (Huang et al., 2015).

2.4 HYSPLIT Calculation

To investigate relationships between the origins of the air masses and the isotopic compositions of S and Hg measured in marine aerosols, 72h back trajectories at 10m have been modeled using HYSPLIT – Hybrid Single Particles Lagrangien Integrated Trajectory- for each day. The model used NCEP-NCAR reanalysis data fields. Back-trajectories for the samples are then incorporated into a map generated by GMT (Generic mapping tools).

3 Hg and S isotopic compositions in marine aerosols

3.1 Hg Results and comparison with literature data

Isotopic compositions of both Hg and S have been measured in this study. The $\delta^{202}Hg$ present a large variation ranging from -1.7‰ to 1.3‰ while the $\Delta^{199}Hg$-values range from -0.89‰ to 0.54‰. The $\Delta^{200}Hg$-values range from -0.06‰ to 0.33‰ and the $\Delta^{201}Hg$-values present a variation from -0.74‰ to 0.63‰. Hg-multiple isotopic compositions measured in this study are compared with the one reported

in the literature both for urban, rural and coastal aerosols (Figure 1) reported in open grey circles, (Das et al., 2016; Fu et al., 2019; Huang et al., 2016; Huang et al., 2019; Huang et al., 2018; Rolison et al., 2013; Xu et al., 2017; Xu et al., 2019; Yu et al., 2016; Yuan et al., 2018).

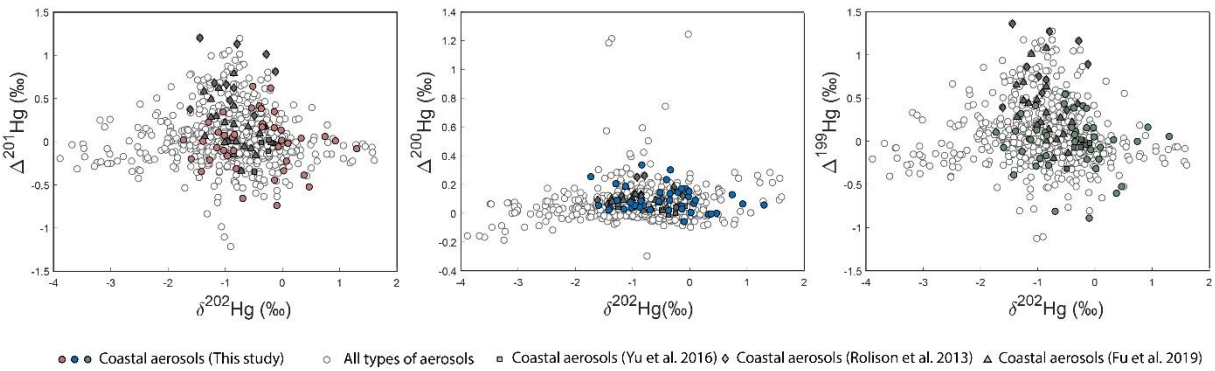

Figure 1: Mercury isotopic compositions in aerosols in a δ^{202}Hg-Δ^{201}Hg diagram, δ^{202}Hg-Δ^{200}Hg diagram and in a δ^{202}Hg-Δ^{199}Hg diagram. Different types of aerosols reported in the literature are also shown.

More specifically, results obtained in this study are compared with aerosols collected in coastal environments in particular the Grand Bay Mississippi (Rolison et al., 2013) in USA, the Dameishan Atmosphere Observatory(Yu et al., 2016) and the Huaniao Island(Fu et al., 2019) in China as no study reports the Hg isotopic compositions on marine aerosols. The Hg isotopic compositions measured on aerosols sampled during this campaign share some characteristics with similar range of Δ^{200}Hg but larger variations of δ^{202}Hg, Δ^{201}Hg and Δ^{199}Hg-values (Figure 1). More precisely, more negative Δ^{201}Hg and Δ^{199}Hg-values are reported in this study, with the lowest values being the same range of variation as the one reported in urban area. This suggests that both urban and coastal aerosols might be affected by the same atmospheric processes.

3.2 S isotopic compositions results and comparison with literature data

The δ^{34}S, Δ^{33}S and Δ^{36}S-values vs V-CDT are presented in Figure 2. The δ^{34}S present a large variation ranging from -2.3‰ to 19.4‰ while the Δ^{33}S-values range from 0.008‰ to 0.441‰ and the Δ^{36}S-values range from -1.2‰ to 0.0‰. The presence of Δ^{33}S-values up to 0.4‰ in marine environment is surprising although no studies reported the S multiple isotopic compositions in marine aerosols in the literature as positive Δ^{33}S values have been reported (Figure 2A) to our knowledge only in urban and rural areas up to 0.5‰(Au Yang et al., 2019; Guo et al., 2010; Han et al., 2017b; Lin et al., 2018b; Romero and Thiemens, 2003; Shaheen et al., 2014) and in Antarctic ice-cores sulfates up to 2‰ (Baroni et al., 2007; Gautier et al., 2018; Hattori et al., 2013; Savarino et al., 2003). Positive Δ^{33}S reported in ice-cores could result from photochemical oxidation of atmospheric SO_2 in the stratosphere that produce high Δ^{33}S-values up to 15‰ (Farquhar et al., 2000; Farquhar et al., 2001; Whitehill et al., 2015; Whitehill and Ono, 2012; Whitehill et al., 2013).

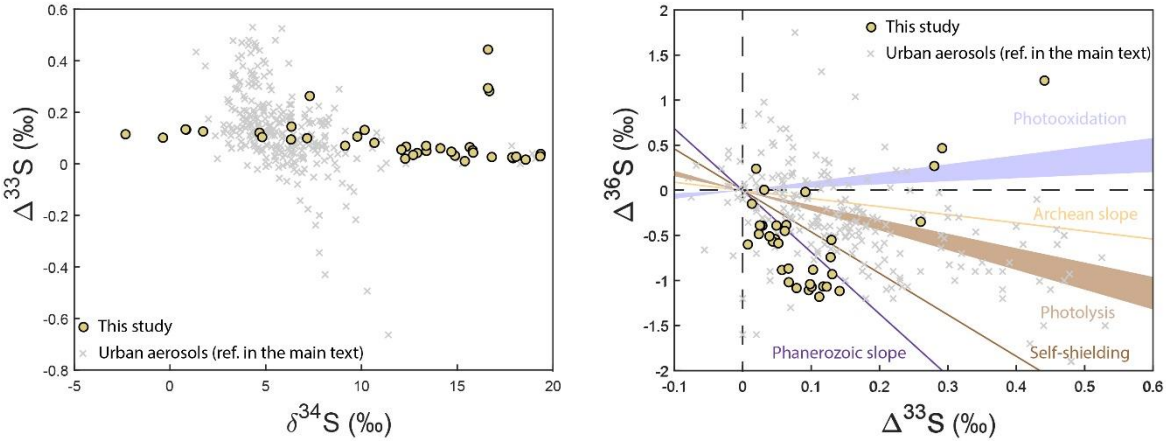

Figure 2 : Sulfur isotopic compositions in a $\delta^{34}S$-$\Delta^{33}S$ diagram and in a $\Delta^{33}S$-$\Delta^{36}S$ diagram. Urban aerosols have also been reported*(Au Yang et al., 2019; Guo et al., 2010; Lin et al., 2018b; Romero and Thiemens, 2003; Shaheen et al., 2014)*. No $\Delta^{33}S$ and $\Delta^{36}S$-values have been reported to our knowledge for marine aerosols. Slopes for the different atmospheric processes (photooxidation, photolysis, self-shielding), Archean slope and Phanerozoic slopes have also been reported.

Thus, stratospheric sulfate aerosols input into the troposphere could be an explanation but according to the three-days HYSPLIT back-trajectory analysis for each sample, none of the samples came from altitudes higher than 2000m for an initial height of 10 or 500m respectively ruling out this hypothesis. SO_2 oxidation by O_2+TMI, OH, H_2O_2/O_3 and NO_2 are also unlikely involved as these oxidation pathways cannot account for these positive $\Delta^{33}S$ up to 0.5‰ (Au Yang et al., 2018; Harris et al., 2013a). Oxidation by halogen compounds would have been another potential candidate. However, the fact that positive $\Delta^{33}S$ have been found in both marine and urban/rural environments suggest that a similar atmospheric processes would occur in both environment. However oxidation of SO_2 by halogen compounds would be important in marine environment, ruling out this hypothesis.

Another study suggested that photooxidation of mineral dust could be responsible for positive $\Delta^{33}S$ although this remains speculative (Au Yang et al., 2019). This hypothesis is consistent with the observation of positive $\Delta^{36}S$-values coupled to positive $\Delta^{33}S$ up to 0.4‰ where both positive $\Delta^{33}S$ and $\Delta^{36}S$ could be produced by photooxidation and photolysis(Whitehill and Ono, 2012) (Figure 2). Moreover, despite conventional crustal references (Fe/Al and K/Al) have not been measured in this study, and knowing that Ca is mostly a carbonate tracer (Formenti et al., 2011), Ca can be used as a dust tracer in this study as Ca/Al ratio in Australian dust varies in a narrow range (i.e. 0.1 to 0.74 (Engelbrecht et al., 2016)). We used the definition of an enrichment factor following :

$$EF(S) = \frac{\left([nss - SO_4]/[Ca]\right)_{particles}}{\left([nss - SO_4]/[Ca]\right)_{soil}}$$

From this definition, we observed an enrichment during the 13/11/2015 to 17/11/2015 (dates which correspond to the $\Delta^{33}S$ positive excursion) with a mean value of 17±7 while the mean EF during the entire cruise is 3 ± 3. This would attest for the implication of dust particles during this period, despite the fact that their contribution cannot be precisely estimated.

Origins of both Hg and S-MIF are discussed in a paper in preparation and submitted soon (with Institute of Geochemistry in 1st affiliation). We will thus not discuss it here.

4 Hg isotopic compositions in an rural and subrural areas

4.1 Sampling strategy

PM_{10} aerosols (particles with an aerodynamical diameter <10 µm) were sampled over a one-year period in 2015 by the RSQA (Réseau de Surveillance de la Qualité de l'Air) in the city of Montreal (45°N 73°W, Canada) and its vicinity. Two monitoring stations (13 and 98) disseminated onto Montreal island were selected for their specific environmental conditions (Figure S1). Station 13 referred as "Drummond" is located downtown and represents the urban background whereas Station 98 referred as "Sainte-Anne de Bellevue" is located at the most western end of the island, in a semi-rural environment under the dominant west-east blowing winds, and thus represents a station less impacted by local anthropogenic atmospheric emissions (Boulet and Melançon, 2012). This sampling strategy was designed to allow comparing a station affected by local anthropogenic emissions and a station where aerosols were expected to have a non-local origin (i.e. aerosols transported to Montreal). In parallel, major pollutant gases, including ozone (O_3), sulfur dioxide (SO_2), nitrogen dioxide (NO_2), as well as $PM_{2.5}$ concentrations were acquired from the Réseau de Surveillance de la Qualité de l'Air (http://ville.montreal.qc.ca/, last access : 02 January 2020).

4.2 Results and Comparison with literature data

Hg-isotopes data have been previously published on aerosols collected in a rural environment in India (Das et al., 2016), in rural, coastal and urban environments in China (Fu et al., 2019; Huang et al., 2016; Huang et al., 2019; Huang et al., 2015; Huang et al., 2018; Xu et al., 2017; Xu et al., 2019; Yu et al., 2016; Yuan et al., 2018) and in a coastal area in the United States (Rolison et al., 2013)

The Hg multiple isotope compositions we measured in aerosols at both stations in Montreal are within the isotope ranges reported in the literature for similar samples (*Figure 4*). It is worth noting that aerosols in Montreal are characterized by negative $\delta^{202}Hg$ and present, to our knowledge, the lowest $\delta^{202}Hg$ ever reported. Aerosols from this study are mainly characterized by low $\Delta^{199}Hg$, close to 0‰, for both the urban and subrural stations. Similarly, they are characterized by very low $\Delta^{200}Hg$, varying from -0.05 to 0.15‰, which is also within the range reported for urban aerosols. Overall, aerosols from Montréal present isotope compositions similar to those of most urban aerosols but different from both rural and coastal aerosols, as they are characterized by an average and 0.29±0.40‰ and 0.39±0.43‰ respectively with a highest value of up to 1.50‰.

Origins of Hg are discussed in a paper already submitted (with Institute of Geochemistry in 1st affiliation). We will thus not discuss it here.

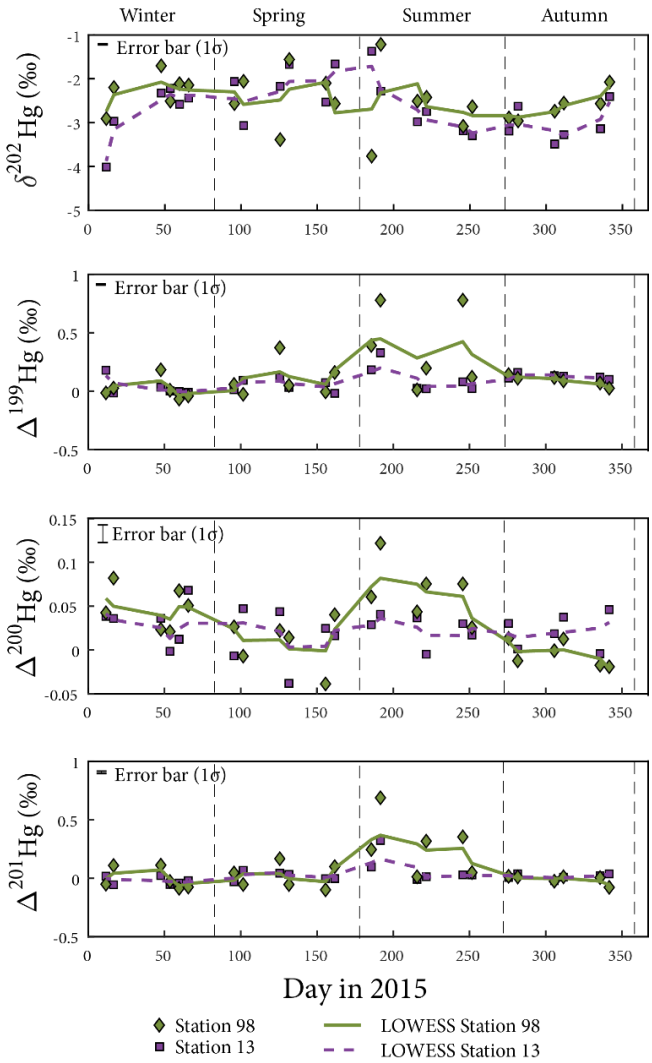

Figure 3: Odd-MIF and even-MIF time series in aerosols sampled in Montreal. Locally weighted scatter plot smoothing (LOWESS) for all the Hg isotopic compositions are also shown

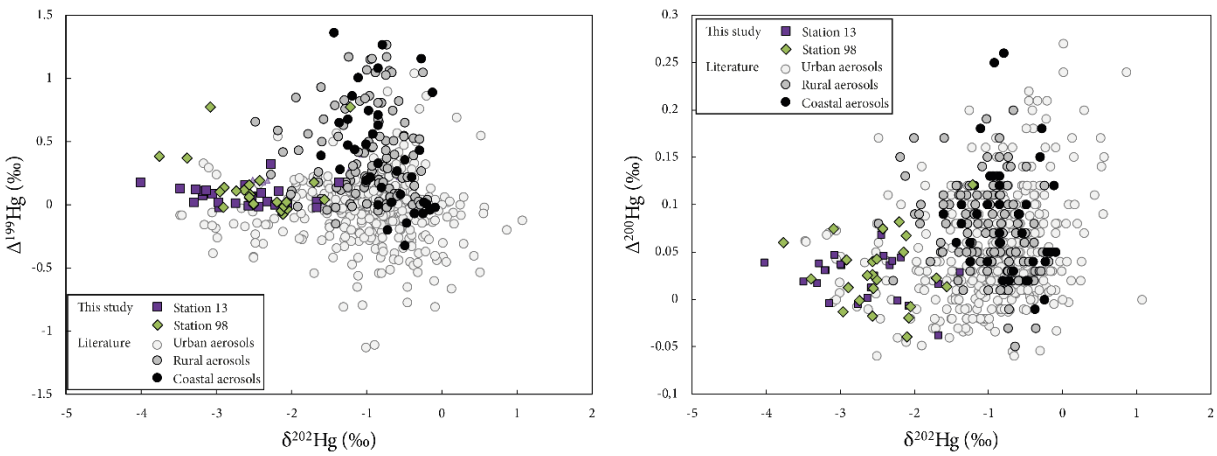

Figure 4 : Variations of (A) Δ^{199}Hg and (B) Δ^{200}Hg as a function of δ^{202}Hg in PBM from PM_{10} aerosols collected in Montreal (purple square and green diamond). Light gray, gray and black dots represent Hg isotopic compositions reported for aerosols from the literatures (Das et al., 2016; Fu et al., 2019; Huang et al., 2016; Huang et al., 2019; Huang et al., 2015; Huang et al., 2018; Rolison et al., 2013; Xu et al., 2017; Xu et al., 2019; Yu et al., 2016; Yuan et al., 2018)

5 S isotopic compositions in an urban area

5.1 Sampling strategy

Aerosols from different size PM_{10} , $PM_{2.5}$ and PM0.5 (particles with an aerodynamical diameter <10 µm, <2.5 µm and <0.5 µm) were sampled over a one-year period in 2018 in the city of Tianjin at the Tianjin University.

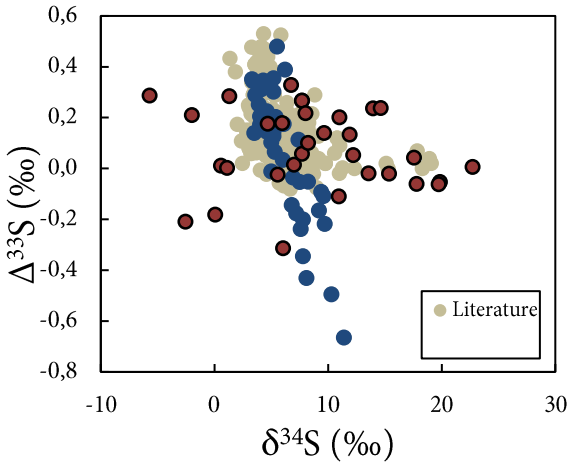

Figure 5 Sulfur isotopic compositions in a $\delta^{34}S$-$\Delta^{33}S$ diagram and in a $\Delta^{33}S$-$\Delta^{36}S$ diagram. Urban aerosols have also been reported (Au Yang et al., 2019; Guo et al., 2010; Han et al., 2017b; Lin et al., 2018b; Romero and Thiemens, 2003; Shaheen et al., 2014)

5.2 S isotopic compositions results and comparison with literature data

The $\delta^{34}S$, $\Delta^{33}S$ vs V-CDT are presented in *Figure 5*. The $\delta^{34}S$ present a large variation ranging from -5.6‰ to 22.3‰ while the $\Delta^{33}S$-values range from -0.318‰ to 0.328‰. We observe that these isotopic compositions are within the range of variation reported in the literature although we observe very negative $\delta^{34}S$ down to -5.6‰ which are scarce (Au Yang et al., 2019; Guo et al., 2010; Han et al., 2017b; Lin et al., 2018b; Romero and Thiemens, 2003; Shaheen et al., 2014). More importantly, we confirm the existence of negative $\Delta^{33}S$ down to -0.3‰ which have been measured only once by Han et al. (2017b) in Beijing aerosols. Again, the observation of such negative $\Delta^{33}S$ occurs mainly in December, which is the same period reported by Han et al. (2017b).

Origin of positive and negative $\Delta^{33}S$ are again not discussed in this report. The paper is in preparation

6 Supplementary activities

6.1 Publications of the thesis papers (1st author and 2nd author)

During this postdoc position, I published two papers from my PhD thesis, one paper is actually in review (ACPD, see below), and am currently writing another paper from my PhD on aerosols combustion (to be submitted soon)

Atmospheric Environment 193 (2018) 109–117

Contents lists available at ScienceDirect

Atmospheric Environment

journal homepage: www.elsevier.com/locate/atmosenv

Atmospheric SO_2 oxidation by NO_2 plays no role in the mass independent sulfur isotope fractionation of urban aerosols

D. Au Yang[a,b,*], G. Bardoux[a], N. Assayag[a], C. Laskar[a], D. Widory[b], P. Cartigny[a]

[a] Laboratoire de Géochimie des Isotopes Stables, Institut de Physique du Globe de Paris, Université Paris Diderot, CNRS UMR 7154, Sorbonne Paris-Cité, 1 rue de Jussieu, 75005, Paris, France

[b] GEOTOP/Université du Québec à Montréal (UQAM), Montréal, H3C 3P8, Canada

Atmos. Chem. Phys., 19, 3779–3796, 2019
https://doi.org/10.5194/acp-19-3779-2019

Atmospheric Chemistry and Physics
Open Access
EGU

Seasonality in the $\Delta^{33}S$ measured in urban aerosols highlights an additional oxidation pathway for atmospheric SO_2

David Au Yang[1,2], Pierre Cartigny[1], Karine Desboeufs[3], and David Widory[2]

[1]Laboratoire de Géochimie des Isotopes Stables, Institut de Physique du Globe de Paris, Université Paris Diderot, CNRS UMR 7154, Sorbonne Paris-Cité, 1 rue de Jussieu, 75005 Paris, France
[2]GEOTOP/Université du Québec à Montreal, Montreal H3C 3P8, Canada
[3]Laboratoire Interuniversitaire des Systèmes Atmosphériques (LISA), UMR7583 CNRS, Université Paris 7 Denis Diderot, Université Paris-Est Créteil, Institut Pierre-Simon Laplace, Créteil, 94010, France

Correspondence: David Au Yang (auyang@mail.gyig.ac.cn)

Received: 12 October 2018 – Discussion started: 17 October 2018
Revised: 25 February 2019 – Accepted: 28 February 2019 – Published: 25 March 2019

https://doi.org/10.5194/acp-2019-971
Preprint. Discussion started: 28 October 2019

Atmospheric Chemistry and Physics Discussions
Open Access
EGU

Oxygen and sulfur mass-independent isotopic signatures in black crusts: the complementary negative $\Delta^{33}S$-reservoir of sulfate aerosols?

Isabelle Genot[1,2], David Au Yang[1,3], Erwan Martin[2], Pierre Cartigny[1], Erwann Legendre[2,4], Marc De Rafelis[5]

[1]Institut de physique du globe de Paris, Université de Paris, CNRS, F-75005 Paris, France.
[2]Sorbonne Université, CNRS-INSU, Institut des Sciences de la Terre de Paris, IsteP UMR7193 Paris, France.
[3]Department of Earth and Planetary Sciences, McGill University, Montréal, Canada.
[4]LATMOS-IPSL - Sorbonne Université - Université Versailles St.-Quentin, Paris, France.
[5]GET, Université Paul Sabatier, Toulouse, France.

Correspondence to: Isabelle Genot (genot@ipgp.fr)

6.2 Publication of papers as coauthor

I also published as a coauthor during my postdoc position (Zhang et al. 2020) and worked with student from prof Chen group members.

Ecotoxicology and Environmental Safety 191 (2020) 110229

Contents lists available at ScienceDirect

Ecotoxicology and Environmental Safety

journal homepage: www.elsevier.com/locate/ecoenv

Mercury isotope compositions in large anthropogenically impacted Pearl River, South China

Yuanyuan Zhang[a,b], Jiubin Chen[a,c,*], Wang Zheng[c], Ruoyu Sun[c], Shengliu Yuan[d], Hongming Cai[c], David Au Yang[a,b], Wei Yuan[c], Mei Meng[c], Zhongwei Wang[a,b], Yulong Liu[a,b], Jianfeng Liu[a,b]

[a] State Key Laboratory of Environmental Geochemistry, Institute of Geochemistry, Chinese Academy of Sciences, Guiyang, Guizhou, 550081, China
[b] University of Chinese Academy of Sciences, Beijing, 100049, China
[c] Institute of Surface-Earth System Science, Tianjin University, Tianjin, 300072, China
[d] Chemistry Department, Trent University, Peterborough, Ontario, K9J7B8, Canada

6.3 Reviewing papers

I also reviewed three papers during this postdoc position

De journalstaff@pnascentral.org
Sujet **PNAS MS# 2018-[redacted] Review Received**
Réponse à rvanvalkenburg@nas.edu
Pour Moi <auyang@ipgp.fr>
Copie à rvanvalkenburg@nas.edu

De editorial@copernicus.org
Sujet **Reminder acp-2018-[redacted] - request for review**
Pour Moi <auyang@mail.gyig.ac.cn>

De Environmental Science & Technology <onbehalfof@manuscriptcentral.com>
Sujet **ES&T manuscript es-2019-[redacted] assigned for review**
Réponse à diamond-office@est.acs.org
Pour Moi <auyang@mail.gyig.ac.cn>
Copie à diamond-office@est.acs.org

6.4 Meeting

I also attended at three conferences

1. **Au Yang D.**, Chen JB., Zheng W., Widory D. (**2019**), Multiple mercury isotopic compositions of aerosols in the atmosphere of Montréal (Canada), American Geophysical Union AGU Fall Meeting, San Francisco, United-State, December 11th 2019 **(Poster)**
2. **Au Yang D.**, Cartigny P., Desboeufs K., Widory D. (**2019**), Seasonality in the $\Delta^{33}S$ measured in urban aerosols highlights an additional oxidation pathway for atmospheric SO_2, 6th Young scientist Forum of Earth Science**s**, Xining, China, October 14th 2019 (**Oral, Invited talk**)
3. **Au Yang D.**, Bardoux G., Widory D., Assayag N., Cartigny P. (**2018**), Atmospheric SO_2 oxidation by NO_2 plays no role in the mass independent sulfur isotope fractionation of urban aerosols, 5th Conference on Earth System Science, Shanghai, Chine, June 3 2018 (**Oral**)

7 Reference

Albrecht, B.A., 1989. Aerosols, cloud microphysics, and fractional cloudiness. Science, 245(4923): 1227-1230.

Alexander, B. et al., 2012. Isotopic constraints on the formation pathways of sulfate aerosol in the marine boundary layer of the subtropical northeast Atlantic Ocean. Journal of Geophysical Research: Atmospheres, 117(D6).

Alexander, B., Park, R., Jacob, D., Gong, S., 2009. Transition metal-catalyzed oxidation of atmospheric sulfur: Global implications for the sulfur budget. Journal of Geophysical Research: Atmospheres, 114(D2).

Au Yang, D. et al., 2018. Atmospheric SO2 oxidation by NO2 plays no role in the mass independent sulfur isotope fractionation of urban aerosols. Atmospheric Environment, 193: 109-117.

Au Yang, D., Cartigny, P., Desboeufs, K., Widory, D., 2019. Seasonality in the Δ33S measured in urban aerosols highlights an additional oxidation pathway for atmospheric SO2. Atmos. Chem. Phys., 19(6): 3779-3796.

Au Yang, D., Landais, G., Assayag, N., Widory, D., Cartigny, P., 2016. Improved analysis of micro-and nanomole-scale sulfur multi-isotope compositions by gas source isotope ratio mass spectrometry. Rapid Communications in Mass Spectrometry, 30(7): 897-907.

Baroni, M., Thiemens, M.H., Delmas, R.J., Savarino, J., 2007. Mass-independent sulfur isotopic compositions in stratospheric volcanic eruptions. Science, 315(5808): 84-87.

Beddows, D.C. et al., 2004. Correlations in the chemical composition of rural background atmospheric aerosol in the UK determined in real time using time-of-flight mass spectrometry. Journal of Environmental Monitoring, 6(2): 124-133.

Benson, D.R., L.-H. Young, F. R. Kameel, and S.-H. Lee, 2008. Laboratory-measured nucleation rates of sulfuric acid and water binary homogeneous nucleation from the SO2 + OH reaction. Geophys. Res. Lett., 35(11).

Bergquist, B.A., Blum, J.D., 2007. Mass-dependent and-independent fractionation of Hg isotopes by photoreduction in aquatic systems. Science, 318(5849): 417-420.

Bieser, J. et al., 2017. Multi-model study of mercury dispersion in the atmosphere: vertical and interhemispheric distribution of mercury species. Atmos. Chem. Phys., 17(11): 6925-6955.

Blum, J.D., Bergquist, B.A., 2007. Reporting of variations in the natural isotopic composition of mercury. Analytical and bioanalytical chemistry, 388(2): 353-359.

Boulet, D., Melançon, S., 2012. Bilan environnemental. Qualité de l'air à Montréal. Rapport Annuel 2011.Ville de Montréal, Service des infrastructures, du transport et de l'environnement, Direction de l'environnement et du développement durable, Division de la planification et du suivi environnemental, RSQA: 8.

Buchachenko, A.L., 2013. Mass-independent isotope effects. The Journal of Physical Chemistry B, 117(8): 2231-2238.

Cai, H., Chen, J., 2016. Mass-independent fractionation of even mercury isotopes. Science bulletin, 61(2): 116-124.

Chen, J., Hintelmann, H., Feng, X., Dimock, B., 2012. Unusual fractionation of both odd and even mercury isotopes in precipitation from Peterborough, ON, Canada. Geochimica et Cosmochimica Acta, 90: 33-46.

Chen, J. et al., 2016. Isotopic evidence for distinct sources of mercury in lake waters and sediments. Chemical Geology, 426: 33-44.

Cheng, Y. et al., 2016. Reactive nitrogen chemistry in aerosol water as a source of sulfate during haze events in China. Science Advances, 2(12): e1601530.

Cohen, M. et al., 2004. Modeling the atmospheric transport and deposition of mercury to the Great Lakes. Environmental Research, 95(3): 247-265.

Das, R. et al., 2016. Mercury isotopes of atmospheric particle bound mercury for source apportionment study in urban Kolkata, India. Elem Sci Anth, 4.

Dauphas, N., Schauble, E.A., 2016. Mass fractionation laws, mass-independent effects, and isotopic anomalies. Annual Review of Earth and Planetary Sciences, 44: 709-783.

De Simone, F. et al., 2015. Model study of global mercury deposition from biomass burning. Environmental science & technology, 49(11): 6712-6721.

Defouilloy, C., Cartigny, P., Assayag, N., Moynier, F., Barrat, J.-A., 2016. High-precision sulfur isotope composition of enstatite meteorites and implications of the formation and evolution of their parent bodies. Geochimica et Cosmochimica Acta, 172: 393-409.

Dibble, T.S., Zelie, M.J., Mao, H., 2012. Thermodynamics of reactions of ClHg and BrHg radicals with atmospherically abundant free radicals. Atmos. Chem. Phys., 12(21): 10271-10279.

Ding, T. et al., 2001. Calibrated sulfur isotope abundance ratios of three IAEA sulfur isotope reference materials and V-CDT with a reassessment of the atomic weight of sulfur. Geochimica et Cosmochimica Acta, 65(15): 2433-2437.

Eldridge, D., Guo, W., Farquhar, J., 2016. Theoretical estimates of equilibrium sulfur isotope effects in aqueous sulfur systems: Highlighting the role of isomers in the sulfite and sulfoxylate systems. Geochimica et Cosmochimica Acta, 195: 171-200.

Engelbrecht, J.P. et al., 2016. Technical note: Mineralogical, chemical, morphological, and optical interrelationships of mineral dust re-suspensions. Atmos. Chem. Phys., 16(17): 10809-10830.

Estrade, N., Carignan, J., Sonke, J.E., Donard, O.F., 2009. Mercury isotope fractionation during liquid–vapor evaporation experiments. Geochimica et Cosmochimica Acta, 73(10): 2693-2711.

Farquhar, J., Bao, H., Thiemens, M., 2000. Atmospheric influence of Earth's earliest sulfur cycle. Science, 289(5480): 756-758.

Farquhar, J., Savarino, J., Airieau, S., Thiemens, M.H., 2001. Observation of wavelength-sensitive mass-independent sulfur isotope effects during SO2 photolysis: Implications for the early atmosphere. Journal of Geophysical Research: Planets (1991–2012), 106(E12): 32829-32839.

Farquhar, J., Wing, B.A., 2003. Multiple sulfur isotopes and the evolution of the atmosphere. Earth and Planetary Science Letters, 213(1): 1-13.

Formenti, P. et al., 2011. Recent progress in understanding physical and chemical properties of African and Asian mineral dust. Atmos. Chem. Phys., 11(16): 8231-8256.

Fu, X. et al., 2019. Domestic and Transboundary Sources of Atmospheric Particulate Bound Mercury in Remote Areas of China: Evidence from Mercury Isotopes. Environmental Science & Technology, 53(4): 1947-1957.

Gautier, E., Savarino, J., Erbland, J., Farquhar, J., 2018. SO2 oxidation kinetics leave a consistent isotopic imprint on volcanic ice core sulfate. Journal of Geophysical Research: Atmospheres.

Gencarelli, C.N., De Simone, F., Hedgecock, I.M., Sprovieri, F., and Pirrone, N., 2014. Development and Application of a Regional-Scale Atmospheric Mercury Model Based on WRF/Chem: A Mediterranean Area Investigation. Environ Sci Pollut Res, 21: 4095.

Geng, H., Yin, R., Li, X., 2018. An optimized protocol for high precision measurement of Hg isotopic compositions in samples with low concentrations of Hg using MC-ICP-MS. Journal of Analytical Atomic Spectrometry, 33(11): 1932-1940.

Giang, A., Selin, N.E., 2016. Benefits of mercury controls for the United States. Proceedings of the National Academy of Sciences, 113(2): 286.

Guo, Z. et al., 2010. Identification of sources and formation processes of atmospheric sulfate by sulfur isotope and scanning electron microscope measurements. Journal of Geophysical Research: Atmospheres, 115(D7).

Han, X. et al., 2017a. Multiple sulfur isotope constraints on sources and formation processes of sulfate in Beijing PM2. 5 aerosol. Environmental Science & Technology.

Han, X. et al., 2017b. Multiple sulfur isotope constraints on sources and formation processes of sulfate in Beijing PM2. 5 aerosol. Environmental science & technology, 51(14): 7794-7803.

Harris, E., Sinha, B., Hoppe, P., Ono, S., 2013a. High-precision measurements of ^{33}S and ^{34}S fractionation during SO_2 oxidation reveal causes of seasonality in SO_2 and sulfate isotopic composition. Environmental science & technology, 47(21): 12174-12183.

Harris, E. et al., 2013b. Enhanced role of transition metal ion catalysis during in-cloud oxidation of SO_2. Science, 340(6133): 727-730.

Hattori, S. et al., 2013. SO2 photoexcitation mechanism links mass-independent sulfur isotopic fractionation in cryospheric sulfate to climate impacting volcanism. Proceedings of the National Academy of Sciences, 110(44): 17656-17661.

Herrmann, H., 2003. Kinetics of aqueous phase reactions relevant for atmospheric chemistry. Chemical reviews, 103(12): 4691-4716.

Horowitz, H.M. et al., 2017. A new mechanism for atmospheric mercury redox chemistry: implications for the global mercury budget. Atmos. Chem. Phys., 17(10): 6353-6371.

Huang, Q. et al., 2016. Isotopic composition for source identification of mercury in atmospheric fine particles. Atmospheric Chemistry and Physics, 16(18): 11773-11786.

Huang, Q. et al., 2019. Diel variation in mercury stable isotope ratios records photoreduction of PM2.5-bound mercury. Atmos. Chem. Phys., 19(1): 315-325.

Huang, Q. et al., 2015. An improved dual-stage protocol to pre-concentrate mercury from airborne particles for precise isotopic measurement. Journal of Analytical Atomic Spectrometry, 30(4): 957-966.

Huang, S. et al., 2018. Natural stable isotopic compositions of mercury in aerosols and wet precipitations around a coal-fired power plant in Xiamen, southeast China. Atmospheric Environment, 173: 72-80.

Kulmala, M. et al., 2004. Formation and growth rates of ultrafine atmospheric particles: a review of observations. Journal of Aerosol Science, 35(2): 143-176.

Labidi, J., Cartigny, P., Birck, J., Assayag, N., Bourrand, J., 2012. Determination of multiple sulfur isotopes in glasses: A reappraisal of the MORB $\delta^{34}S$. Chemical Geology, 334: 189-198.

Lee, Y.N., Schwartz, S.E., 1983. Kinetics of oxidation of aqueous sulfur (IV) by nitrogen dioxide. Precipitation Scavenging, Dry Deposition, and Resuspension, 1.

Lelieveld, J., Evans, J., Fnais, M., Giannadaki, D., Pozzer, A., 2015. The contribution of outdoor air pollution sources to premature mortality on a global scale. Nature, 525(7569): 367-371.

Levy, H. et al., 2013. The roles of aerosol direct and indirect effects in past and future climate change. Journal of Geophysical Research: Atmospheres, 118(10): 4521-4532.

Lin, M. et al., 2018a. Atmospheric sulfur isotopic anomalies recorded at Mt. Everest across the Anthropocene. Proceedings of the National Academy of Sciences, 115(27): 6964-6969.

Lin, M. et al., 2018b. Five-S-isotope evidence of two distinct mass-independent sulfur isotope effects and implications for the modern and Archean atmospheres. Proceedings of the National Academy of Sciences, 115(34): 8541-8546.

Mead, C., Lyons, J.R., Johnson, T.M., Anbar, A.D., 2013. Unique Hg Stable Isotope Signatures of Compact Fluorescent Lamp-Sourced Hg. Environmental Science & Technology, 47(6): 2542-2547.

Mertes, S. et al., 2005a. Evolution of particle concentration and size distribution observed upwind, inside and downwind hill cap clouds at connected flow conditions during FEBUKO. Atmospheric Environment, 39(23): 4233-4245.

Mertes, S., Lehmann, K., Nowak, A., Massling, A., Wiedensohler, A., 2005b. Link between aerosol hygroscopic growth and droplet activation observed for hill-capped clouds at connected flow conditions during FEBUKO. Atmospheric Environment, 39(23): 4247-4256.

Myhre, G. et al., 2013. Anthropogenic and natural radiative forcing. Climate change, 423.

Ono, S., Whitehill, A., Lyons, J., 2013. Contribution of isotopologue self-shielding to sulfur mass-independent fractionation during sulfur dioxide photolysis. Journal of Geophysical Research: Atmospheres, 118(5): 2444-2454.

Otake, T., Lasaga, A.C., Ohmoto, H., 2008. Ab initio calculations for equilibrium fractionations in multiple sulfur isotope systems. Chemical Geology, 249(3): 357-376.

Paris, R., Desboeufs, K., Formenti, P., Nava, S., Chou, C., 2010. Chemical characterisation of iron in dust and biomass burning aerosols during AMMA-SOP0/DABEX: implication for iron solubility. Atmospheric Chemistry and Physics, 10(9): 4273-4282.

Penner, J.E., Dickinson, R.E., O'Neill, C.A., 1992. Effects of aerosol from biomass burning on the global radiation budget. Science, 256(5062): 1432-1434.

Penner, J.E. et al., 2006. Model intercomparison of indirect aerosol effects. Atmospheric Chemistry and Physics, 6(11): 3391-3405.

Ramanathan, V. et al., 2005. Atmospheric brown clouds: Impacts on South Asian climate and hydrological cycle. Proceedings of the National Academy of Sciences of the United States of America, 102(15): 5326-5333.

Ramanathan, V., Crutzen, P.J., Kiehl, T.J., Rosenfeld, D., 2001. Aerosols, Climate, and the Hydrological Cycle. Science, 294: 2119-2124.

Rolison, J.M., Landing, W.M., Luke, W., Cohen, M., Salters, V.J.M., 2013. Isotopic composition of species-specific atmospheric Hg in a coastal environment. Chemical Geology, 336: 37-49.

Romero, A.B., Thiemens, M.H., 2003. Mass-independent sulfur isotopic compositions in present-day sulfate aerosols. Journal of Geophysical Research: Atmospheres (1984–2012), 108(D16).

Sarwar, G. et al., 2013. Potential impacts of two SO 2 oxidation pathways on regional sulfate concentrations: aqueous-phase oxidation by NO 2 and gas-phase oxidation by Stabilized Criegee Intermediates. Atmospheric environment, 68: 186-197.

Savarino, J., Romero, A., Cole-Dai, J., Bekki, S., Thiemens, M., 2003. UV induced mass-independent sulfur isotope fractionation in stratospheric volcanic sulfate. Geophysical Research Letters, 30(21).

Seinfeld, J.H., Pandis, S.N., 2012. Atmospheric chemistry and physics: from air pollution to climate change. John Wiley & Sons.

Selin, N.E., 2009. Global Biogeochemical Cycling of Mercury: A Review. Annual Review of Environment and Resources, 34(1): 43-63.

Shaheen, R. et al., 2014. Large sulfur-isotope anomaly in nonvolcanic sulfate aerosol and its implications for the Archean atmosphere. Proceedings of the National Academy of Sciences, 111(33): 11979-11983.

Sherman, L.S. et al., 2010. Mass-independent fractionation of mercury isotopes in Arctic snow driven by sunlight. Nature Geoscience, 3(3): 173.

Si, L., Ariya, P.A., 2018. Recent Advances in Atmospheric Chemistry of Mercury. Atmosphere, 9(2): 76.

Sun, G. et al., 2016. Mass-dependent and-independent fractionation of mercury isotope during gas-phase oxidation of elemental mercury vapor by atomic Cl and Br. Environmental science & technology, 50(17): 9232-9241.

Sun, R., Enrico, M., Heimbürger, L.-E., Scott, C., Sonke, J.E., 2013. A double-stage tube furnace—acid-trapping protocol for the pre-concentration of mercury from solid samples for isotopic analysis. Analytical and bioanalytical chemistry, 405(21): 6771-6781.

Tanaka, N., Rye, D.M., Xiao, Y., Lasaga, A.C., 1994. Use of stable sulfur isotope systematics for evaluating oxidation reaction pathways and in-cloud-scavenging of sulfur dioxide in the atmosphere. Geophysical research letters, 21(14): 1519-1522.

Thode, H., Monster, J., Dunford, H., 1961. Sulphur isotope geochemistry. Geochimica et Cosmochimica Acta, 25(3): 159-174.

Travnikov, O. et al., 2017. Multi-model study of mercury dispersion in the atmosphere: atmospheric processes and model evaluation. Atmos. Chem. Phys., 17(8): 5271-5295.

Walters, D.M. et al., 2015. Methylmercury Bioaccumulation in Stream Food Webs Declines with Increasing Primary Production. Environmental Science & Technology, 49(13): 7762-7769.

Wang, Z. et al., 2015. Mass-dependent and mass-independent fractionation of mercury isotopes in precipitation from Guiyang, SW China. Comptes Rendus Geoscience, 347(7): 358-367.

Watanabe, Y., Farquhar, J., Ohmoto, H., 2009. Anomalous fractionations of sulfur isotopes during thermochemical sulfate reduction. Science, 324(5925): 370-373.

Whitehill, A., Jiang, B., Guo, H., Ono, S., 2015. SO 2 photolysis as a source for sulfur mass-independent isotope signatures in stratospehric aerosols. Atmospheric Chemistry and Physics, 15(4): 1843-1864.

Whitehill, A.R., Ono, S., 2012. Excitation band dependence of sulfur isotope mass-independent fractionation during photochemistry of sulfur dioxide using broadband light sources. Geochimica et Cosmochimica Acta, 94: 238-253.

Whitehill, A.R. et al., 2013. Vibronic origin of sulfur mass-independent isotope effect in photoexcitation of SO2 and the implications to the early earth's atmosphere. Proceedings of the National Academy of Sciences, 110(44): 17697-17702.

Xu, H. et al., 2017. Seasonal and Annual Variations in Atmospheric Hg and Pb Isotopes in Xi'an, China. Environmental Science & Technology, 51(7): 3759-3766.

Xu, H.M. et al., 2019. Mercury stable isotope compositions of Chinese urban fine particulates in winter haze days: Implications for Hg sources and transformations. Chemical Geology, 504: 267-275.

Yin, R. et al., 2016. Effects of mercury and thallium concentrations on high precision determination of mercury isotopic composition by Neptune Plus multiple collector inductively coupled plasma mass spectrometry. Journal of Analytical Atomic Spectrometry, 31(10): 2060-2068.

Young, E.D., Galy, A., Nagahara, H., 2002. Kinetic and equilibrium mass-dependent isotope fractionation laws in nature and their geochemical and cosmochemical significance. Geochimica et Cosmochimica Acta, 66(6): 1095-1104.

Yu, B. et al., 2016. Isotopic Composition of Atmospheric Mercury in China: New Evidence for Sources and Transformation Processes in Air and in Vegetation. Environmental Science & Technology, 50(17): 9262-9269.

Yuan, S. et al., 2018. Sequential samples reveal significant variation of mercury isotope ratios during single rainfall events. Science of the total environment, 624: 133-144.

Yuan, S. et al., 2015. Large variation of mercury isotope composition during a single precipitation event at Lhasa City, Tibetan Plateau, China. Procedia Earth and Planetary Science, 13: 282-286.

Zhang, Y. et al., 2020. Mercury isotope compositions in large anthropogenically impacted Pearl River, South China. Ecotoxicology and Environmental Safety, 191: 110229.

Zheng, W., Hintelmann, H., 2009. Mercury isotope fractionation during photoreduction in natural water is controlled by its Hg/DOC ratio. Geochimica et Cosmochimica Acta, 73(22): 6704-6715.

Zheng, W., Hintelmann, H., 2010. Isotope fractionation of mercury during its photochemical reduction by low-molecular-weight organic compounds. The Journal of Physical Chemistry A, 114(12): 4246-4253.